"Yeast Pmp3p has an important role in plasma membrane organization."

De Block, Julien ; Szopinska, Aleksandra ; Guerriat, Bérengère ; Dodzian, Joanna ; Villers, Jennifer ; Hochstenbach, Jean-François ; Morsomme, Pierre

Abstract

Pmp3p-related proteins are highly conserved proteins that exist in bacteria, yeast, nematodes and plants, and its transcript is regulated in response to abiotic stresses, such as low temperature or high salinity. Pmp3p was originally identified in Saccharomyces cerevisiae, and it belongs to the sensitive to Na(+) (SNA)-protein family, which comprises four members - Pmp3p/Sna1p, Sna2p, Sna3p and Sna4p. Deletion of the PMP3 gene conferred sensitivity to cytotoxic cations, whereas removal of the other SNA genes did not lead to clear phenotypic effects. It has long been believed that Pmp3p-related proteins have a common and important role in the modulation of plasma membrane potential and in the regulation of intracellular ion homeostasis. Here, we show that several growth phenotypes linked to PMP3 deletion can be modulated by the removal of specific genes involved in sphingolipid synthesis. These genetic interactions, together with lipid binding assays and epifluorescence microscopy, as...

Document type : *Article de périodique (Journal article)*

Référence bibliographique

De Block, Julien ; Szopinska, Aleksandra ; Guerriat, Bérengère ; Dodzian, Joanna ; Villers, Jennifer ; et. al. *Yeast Pmp3p has an important role in plasma membrane organization.*. In: *Journal of Cell Science*, Vol. 128, no.19, p. 3646-3659 (2015)

DOI : 10.1242/jcs.173211

© 2015. Published by The Company of Biologists Ltd | Journal of Cell Science (2015) 128, 3646-3659 doi:10.1242/jcs.173211

RESEARCH ARTICLE

Yeast Pmp3p has an important role in plasma membrane organization

Julien De Block, Aleksandra Szopinska, Bérengère Guerriat, Joanna Dodzian, Jennifer Villers, Jean-François Hochstenbach and Pierre Morsomme*

ABSTRACT

Pmp3p-related proteins are highly conserved proteins that exist in bacteria, yeast, nematodes and plants, and its transcript is regulated in response to abiotic stresses, such as low temperature or high salinity. Pmp3p was originally identified in *Saccharomyces cerevisiae*, and it belongs to the sensitive to Na^+ (SNA)-protein family, which comprises four members – Pmp3p/Sna1p, Sna2p, Sna3p and Sna4p. Deletion of the *PMP3* gene conferred sensitivity to cytotoxic cations, whereas removal of the other *SNA* genes did not lead to clear phenotypic effects. It has long been believed that Pmp3p-related proteins have a common and important role in the modulation of plasma membrane potential and in the regulation of intracellular ion homeostasis. Here, we show that several growth phenotypes linked to *PMP3* deletion can be modulated by the removal of specific genes involved in sphingolipid synthesis. These genetic interactions, together with lipid binding assays and epifluorescence microscopy, as well as other biochemical experiments, suggest that Pmp3p could be part of a phosphoinositide-regulated stress sensor.

KEY WORDS: Proteolipid, SNA, Phosphoinositide, Sphingolipid

INTRODUCTION

Phosphoinositides represent only a small fraction of phospholipids, but they are important signaling molecules. They are products of 3′, 4′ and 5′ phosphorylation on the inositol in all of the possible combinations of the structural lipid phosphatidylinositol. These molecules are localized along the secretory and endocytic pathways, as well as in the nucleus in eukaryotes (Shah et al., 2013). They regulate various structural and developmental functions in all eukaryotic models, such as membrane biogenesis, lipid homeostasis, vesicular trafficking, and cytoskeleton organization and dynamic (D'Angelo et al., 2008; Ischebeck et al., 2010; Saarikangas et al., 2010).

In the yeast *Saccharomyces cerevisiae*, the reduction of phosphatidylinositol-4,5-bisphosphate [PI(4,5)P_2] abundance through the inactivation of the only yeast plasma membrane phosphatidylinositol-4-phosphate [PI(4)*P*] kinase, Mss4p, reduces the plasma membrane association of Pil1p and Lsp1p (Karotki et al., 2011). Pil1p and Lsp1p, two abundant homologous proteins, and several other proteins of yet unknown functions (Aguilar et al., 2010) form large cytosolic complexes called eisosomes (Walther et al., 2006). These complexes are associated with furrow-like invaginations of the plasma membrane (Stradalova et al., 2009).

Université Catholique de Louvain, Institut des Sciences de la Vie, Croix du Sud 4-5, Louvain-la-Neuve B-1348, Belgium.

*Author for correspondence (pierre.morsomme@uclouvain.be)

Received 22 April 2015; Accepted 18 August 2015

Both Pil1p and Lsp1p contain a Bin1-amphiphysin-Rvs161/167 (BAR) domain that is positively charged (Olivera-Couto et al., 2011). These domains are necessary for Pil1p and Lsp1p to tubulate into helical half cylinders to mold the furrow invaginations (Stradalova et al., 2009; Karotki et al., 2011). The association of Pil1p and Lsp1p with the plasma membrane is likely to be mediated through their short N-terminal protein segment, as well as through the binding of their positively charged BAR domain with negatively charged lipids from the plasma membrane, such as phosphoinositides. Membrane organization by eisosomes is important for the detection of the levels of the sphingolipid precursors phytosphingosine (PHS) and dihydrosphingosine (DHS) (Frohlich et al., 2009). Pil1p specifically recruits the PI(4,5)P_2 phosphatase Inp51/Sjl1 to the plasma membrane, and is crucial for maintaining normal plasma membrane phosphoinositide levels and availability (Frohlich et al., 2014).

Phosphoinositide regulation is also essential at the vacuole. Atg18p binds to both phosphatidylinositol-3-phosphate [PI(3)*P*] and phosphatidylinositol-3,5-bisphosphate [PI(3,5)P_2]. Binding to PI(3)*P* is essential to autophagy, whereas binding to PI(3,5)P_2 is essential for vacuolar morphology (Obara et al., 2008). Autophagy is a system that internalizes bulk cellular compartments into lytic compartments when cells undergo nutrient starvation. In the yeast *S. cerevisiae*, autophagosome formation starts at the pre-autophagosomal structure (PAS), which can be observed as punctae proximal to the vacuole (Suzuki et al., 2001). Atg18, similar to other Atg-family proteins, localizes, at least partially, into the PAS (Suzuki et al., 2013).

The Pmp3/Sna family is present in bacteria, nematodes and plants, but is not present in mammals. The function of these genes has not yet been resolved. Orthologs from barley (Goddard et al., 1993), rice (Morsy et al., 2005), *Arabidopsis thaliana* (Medina et al., 2001) and *Aneurolepidium chinense* (Inada et al., 2005) are stimulated during salt and oxidative stress, and when exposed to low temperatures. The *RCI2A* gene from *A. thaliana* can functionally replace *PMP3* in *S. cerevisiae* (Navarre and Goffeau, 2000; Nylander et al., 2001). Plasma membrane proteolipid 3 (Pmp3p) from *S. cerevisiae*, which gives the name to the family, was found through chloroform–methanol extraction of purified plasma membranes (Navarre et al., 1992, 1994; Navarre and Goffeau, 2000). This protein of 55 amino acids with two transmembrane domains has the same properties as proteolipids, even though a direct link with a lipid has not been shown. Three homologs are present in yeast: Sna2p, Sna3p and Sna4p. Those three are respectively present at the vacuole membrane, lumen and both locations (Reggiori and Pelham, 2001; Stawiecka-Mirota et al., 2007; Pokrzywa et al., 2009; Renard et al., 2010). The *SNA3* gene is in tandem with *INO1*, and the pattern of inositol-mediated regulation of the *SNA3–INO1* tandem genes is similar (Shetty et al., 2013). None of the *SNA* genes are essential. Only mutation of Pmp3p has some known phenotypes.

Journal of Cell Science

Journal of Cell Science (2015) 128, 3646-3659 doi:10.1242/jcs.173211

The deletion of *PMP3* induces sensitivity to NaCl, hygromycin B, tetramethylammonium (Navarre and Goffeau, 2000) and amphotericin B (Huang et al., 2013). The NaCl phenotype cannot be explained through an effect on the two major Na^+ expelling pumps, because *pmr2Δ nha1Δ* Na^+ sensitivity is exacerbated when *PMP3* is deleted (Navarre and Goffeau, 2000). Amphotericin B is a polyene that binds to ergosterol and forms transmembrane pores on the cell membrane, leading to leakage of the cellular contents and cell death (Dennis et al., 1970; Bolard, 1986). Huang et al. suggest that Pmp3p antagonizes the ergosterol-binding effect of amphotericin B, probably by preventing the insertion of amphotericin B into the plasma membrane (Huang et al., 2013). A recent study has shown that the amphotericin-B-treated phenotype of *pmp3Δ* can be modulated through the sphingolipid pathway (Bari et al., 2015). Reports by Bari et al. and Huang et al. both rule out an increase in ergosterol content as the source of the sensitivity to amphotericin B. In addition, Bari et al. show that the salt sensitivity of *pmp3Δ* can be suppressed by overexpressing *SUR7*. Sur7p is an integral plasma membrane protein that affects the sphingolipid composition of the plasma membrane (Young et al., 2002) and is localized at eisosome apposed sites (Walther et al., 2006). A *pmp3Δ* strain is slightly resistant to the polyamine spermine (Erez and Kahana, 2002). A genome-wide study has revealed that the *pmp3Δ* strain is sensitive to the triterpene neothyonidioside (Yibmantasiri et al., 2012), which binds directly to ergosterol. The authors suggest that a threshold of ergosterol concentration is required for its toxicity. Another genome-wide study has revealed *pmp3Δ* as a sensitive strain for a toxic amyloid structure, M8 (Couthouis et al., 2010). Amyloids are proteins that segregate together to form quaternary structures called amyloid fibrils, which can lead to various diseases (Hammer et al., 2008). Couthouis et al. suggest that the toxicity of M8 comes from its propensity to be inserted in phospholipid membranes and to hamper membrane fission, leading to vesicular trafficking poisoning, mostly at the endosome and vacuole (Couthouis et al., 2010). Munkacsi et al. have shown that the double deletion mutant *pmp3Δ ncr1Δ* has a growth defect when grown under anaerobic conditions compared to the single deletion mutants and the wild type (Munkacsi et al., 2011). *NCR1* has been suggested to be responsible for mannose-inositol-phosphoceramide (MIPC) recycling out of the vacuole (Malathi et al., 2004).

Here, we found genetic interactions between *PMP3* and specific genes involved in sphingolipid synthesis. These genetic interactions, together with lipid-binding assays and epifluorescence microscopy, as well as other biochemical experiments, indicate that Pmp3p is part of a phosphoinositide-regulated stress sensor.

RESULTS

Absence of *PMP3* induces changes in protein abundance at the plasma membrane

PMP3 is the only gene of the Sna family that, when deleted, results in an observable phenotype. We postulated that some aspects of this phenotype could be explained by a modification of the abundance of some plasma membrane proteins. We performed a proteomic analysis by using mass spectrometry to analyze purified plasma membranes from wild-type and *pmp3Δ* yeast strains that had been grown to an optical density at 600 nm of 3 (OD_{600}=3), which is the minimum amount of cells required for the analysis. Plasma membranes were purified as described previously (Szopinska et al., 2011). The purification procedure was followed by measuring the relative enrichment of Pma1p, the plasma membrane H^+-ATPase, compared to that of markers of the endoplasmic reticulum (ER) (Sec22p), Golgi complex (Emp47p), endosomes (Pep12p) and cytosol (Cdc48p) (supplementary material Fig. S1). Plasma membrane proteins were digested with trypsin, and the peptides were separated and identified with liquid chromatography and tandem mass spectrometry (LC MS/MS), leading to the identification of 120 plasma membrane proteins. Among them, 59% were integral plasma membrane proteins, 20% were lipid-anchored and 21% are known to be tightly associated with the plasma membrane. Plasma membrane enrichment was confirmed by the relative abundance of peptides originating from plasma membrane proteins compared to other organelles (supplementary material Table S5). The comparison between wild type and *pmp3Δ* was performed by using isobaric tagging for relative and absolute quantification (iTraq) labeling, an isobaric labeling method used in quantitative proteomics (tandem mass spectrometry) to determine the amount of proteins from different sources in a single experiment (Ross et al., 2004). This method allowed for the detection of 14 statistically reproducible differences in protein amounts (Fig. 1, supplementary material Table S1). When *PMP3* was deleted, we observed a decrease ranging from 16 to 30% in the amount of the following membrane-associated proteins compared to that in the wild type: Ena1p and/or Ena2p (Na^+ transporters), Pdr5p and Snq2p (ATP-binding cassette transporters), Zeo1p (cell wall stress sensor), Ftr1p and Fet4p (iron transporters), Hxt3p (hexose transporter), Crh2p (chitin transglycosylase) and Ylr413wp [a predicted integral membrane protein paralogous to *Fat3p* – a protein required for fatty acid uptake (Faergeman et al., 1997)]. Conversely, we observed an increase of abundance from 17 to 59% in *pmp3Δ* for proteins involved in endocytosis: End3p (+59%), Sla1p (+27%), Sla2p (+42%), Ede1p (+17%) and Pan1p (+35%). Ede1p and Sla2p are recruited to the future endocytosis point earlier than Sla1p, End3p and Pan1p, which form an actin-cytoskeleton-regulatory complex (Tang et al., 2000; Carroll et al., 2012).

The BY4742 strain used for this proteomic analysis has three *ENA* genes in the *PMR2* locus: *ENA1*, *ENA2* and *ENA5*. Owing to the similarity between Ena1p and Ena2p, which differ only in thirteen amino acids, no peptide is able to discriminate between them as they share more than 97% identity (therefore referred to as Ena1/2p below). The Ena1p gene was more likely to have been detected here owing to its higher abundance in this strain (Garciadeblas et al., 1993). This alone cannot explain the sensitivity to Na^+, because a *pmr2Δ nha1Δ* strain still exhibits an increased sensitivity to Na^+ when *PMP3* is deleted (Navarre and Goffeau, 2000). We confirmed the results of the proteomic analysis by immunoblotting total protein extracts of selected strains in which the genes of interest had been tagged with a 6× hemagglutinin (6HA) tag (Fig. 1B,C). This method allowed for confirmation (compared to purified plasma membrane) of the effect of *PMP3* deletion on Ena1/2p, Pdr5p, Zeo1p, Sla1p, Sla2p, Ede1p and Pan1p. The transformation method used to add the 6HA tag requires a sequence homology of 45 base pairs. As *ENA1* and *ENA2* share the exact same C-terminus, the tagging method could not discriminate the two homologs. Both genes were thus tagged in the genome. The insolubility of Crh2p and Ylr413wp prevented us from quantifying their relative amounts. Snq2p did not show any differences in the total cell level. Ena1p and Ena2p (*PMR2* locus) are known to be Na^+ transporters, and null mutants of *PDR5* and *SNQ2* are sensitive to Na^+ (Miyahara et al., 1996). Our proteomic analysis showed a decrease in Ena1/2p, Pdr5p and Snq2p. Nonetheless, the absence of *PMP3* still enhanced the sensitivity to salt in a *pmr2Δ nha1Δ vnx1Δ pdr5Δ snq2Δ* strain (supplementary material Fig. S2).

Journal of Cell Science (2015) 128, 3646-3659 doi:10.1242/jcs.173211

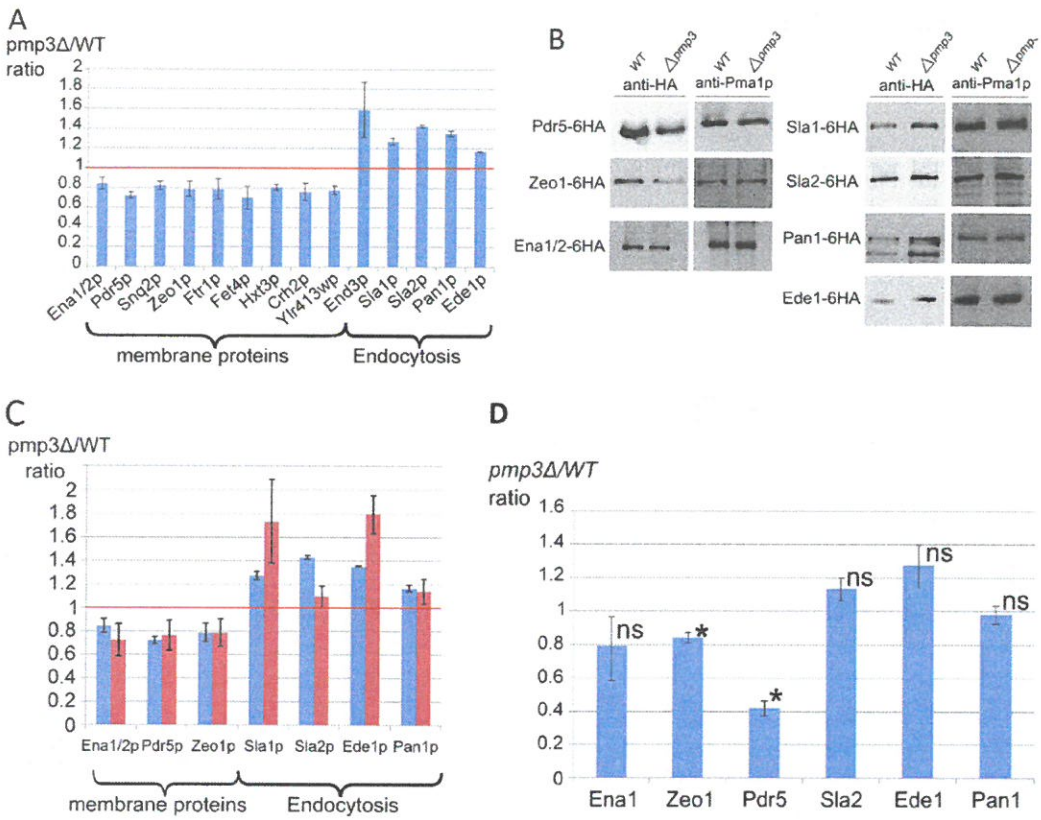

Fig. 1. Deletion of *PMP3* induces a decrease of plasma membrane proteins and an increase of endocytosis proteins compared to the wild type in purified plasma membranes. (A) iTraq analysis of purified plasma membranes from wild-type (WT) and *pmp3Δ S. cerevisiae* BY4742 strains are shown as the ratio of the quantity of proteins of the deletion mutant over the WT strain taken at OD_{600}=3 for three independent repeats. Error bars represent the s.d. of the mean of the ratios. All of the results shown are different from 1 according to a two-tailed *t*-test at *P*-value of 0.05. (B) Validation of quantitative proteomics data by immunoblotting. Immunodetection of HA-tagged target proteins extracted from the WT and *pmp3Δ* strains. Immunodetection was performed to detect Pma1p as a loading control for normalization of data. (C) Comparison between the quantitative proteomics (blue) and immunodetection (red) results. Error bars show the s.d. from at least three independent repeats. (D) Transcription is reduced by 60% in the *pmp3Δ* strain compared to the WT. Results are shown as the qRT-PCR ratio of the quantity of the indicated mRNA in *pmp3Δ* over that in the WT strain. cDNA levels were normalized to the geometric mean of *UBC6*, *TAF10* and *ALG9* mRNA amounts extracted at $OD_{600\,nm}$=0.25. Error bars represent the s.d. from the three repeats. Each ratio was compared to 1 by using a two-tailed *t*-test (ns, not statistically different from 1; **P*<0.05).

PDR5 is downregulated in *pmp3Δ*

To ascertain if the difference in protein amount arose through transcriptomic regulation, we performed a quantitative reverse-transcriptase (qRT)-PCR analysis on the target genes that had been validated with immunoblotting. Results were normalized by using a geometric mean of the amounts of mRNA of *UBC6, TAF10* and *ALG9*, which are the most stable under those conditions (Teste et al., 2009). The results showed that *PDR5* was downregulated by 60% (Fig. 1D). A small decrease was also observed for *ZEO1*. No statistical differences were observed for the remaining genes.

PMP3 deletion has an effect on phosphorylation and localization of Pil1p

Under normal growth conditions, the pool of Pil1 protein is divided between the plasma membrane in eisosome patches (dephosphorylated state) and the cytosol (phosphorylated state) (Walther et al., 2007). Eisosomes are cytosolic complexes of soluble proteins that are in contact with plasma membrane microdomains which are enriched in ergosterol (called MCCs) (Grossmann et al., 2008). Endocytosis events do not take place in the microdomain MCC, but in the ER-free zone of the plasma membrane (Stradalova et al., 2012). Pil1p influences the cortical ER network spreading (Stradalova et al., 2012) and is involved in the recruitment of endocytic proteins (Aguilar et al., 2010; Murphy et al., 2011). We questioned how Pil1p behaved when *PMP3* is absent. Total extracts and purified plasma membrane fractions were analyzed by immunoblotting using antibodies against Pil1. A phosphorylated band was visible in wild-type crude extracts. This band was lost when total extracts were treated with phosphatase and was not visible in purified plasma membrane fractions. Interestingly, the phosphorylation of Pil1p in the *pmp3Δ* strain was not detected in total cell extracts (Fig. 2A). To confirm these results, we observed the localization of green fluorescent protein (GFP-tagged) Pil1 (Pil1–GFP) in a wild-type strain that was devoid or not of Pmp3p. We observed that Pil1–GFP localized in fewer eisosomes near to the plasma membrane in a *pmp3Δ* strain (Fig. 2B). The relative intensity of the fluorescence per eisosome was 60% higher in the *pmp3Δ* strain compared to that of the wild type. Moreover, the size of the eisosomes seemed larger, although the epifluorescence microscope did not allow for precise measurements of the size of fluorescent spots. This result shows that a lack of *PMP3* has an effect on Pil1p regulation and on eisosome organization, and it indicates that there is an excess of precursors of complex sphingolipids [long chain

Journal of Cell Science (2015) 128, 3646-3659 doi:10.1242/jcs.173211

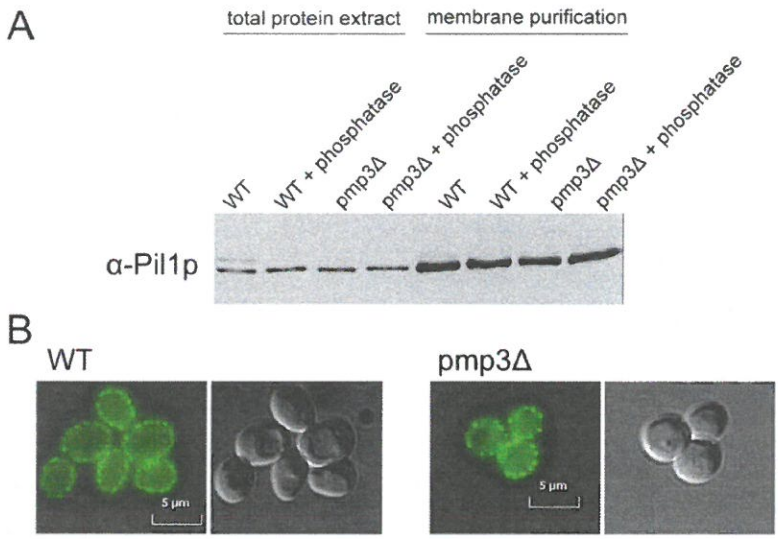

Fig. 2. The absence of Pmp3p modifies Pil1p phosphorylation and assembly to the eisosomes. (A) Immunodetection of Pil1p using a polyclonal antibody in wild-type (WT) and *pmp3Δ* total protein extracts and purified plasma membranes (10 µg of proteins) incubated with or without phosphatase λ. (B) Location of Pil1–GFP (green) in the WT (left) and *pmp3Δ* (right) strains grown to OD_{600}=3. Quantification of the number of eisosomes on the mid-section of 100 cells (three repeats) gave an average of 18.4±0.3 eisosomes for the WT and 13.2±0.3 eisosomes for *pmp3Δ*.

bases (LCB)], enhancing Pil1p dephosphorylation. Interestingly, Bari et al. have shown that the overexpression of *SUR7*, coding for an eisosome protein, is sufficient to rescue the *pmp3Δ* sensitive-to-NaCl phenotype.

PMP3 has an endocytosis defect

Because the proteomic analysis showed a decrease in specific membrane proteins and an increase in endocytosis proteins, we wondered whether endocytosis itself is changed by the deletion of *PMP3*. In addition, a previous study has shown that eisosomes might play a role in endocytosis (Walther et al., 2006). Those authors monitored the time course of FM4-64 internalization in the wild-type and *pil1Δ* strains, and show that deletion of *PIL1* decreased the rate of endocytosis. We reproduced this FM4-64 uptake experiment using the wild-type, *pil1Δ* and *pmp3Δ* strains. We labeled the cells with FM4-64 as described in the Materials and Methods. The FM4-64 signal intensity in the vacuolar membrane of the wild-type and *pmp3Δ* strains was very similar; however, many foci were still seen after 50 min of chase in the *pmp3Δ* strain, but not in the wild type (Fig. 3). These results suggest that there is a delay in FM4-64 endocytosis in *pmp3Δ* compared to the wild type.

The eisosomes are associated with plasma membrane microdomains that contain at least nine integral membrane proteins, including Can1p and Sur7p. In order to test whether Pmp3p controls the stability of transporters located in these microdomains, we monitored Can1p–GFP and Sur7p–GFP turnover in wild-type and *pmp3Δ* strains in the presence of cycloheximide. The basal turnover of Can1p was slower in the *pmp3Δ* strain compared to that the wild type. In the wild type, the intensity of the band corresponding to Can1p–GFP decreased from 30% and 75% after 30 and 60 min, respectively. By contrast, the signal was more stable in the *pmp3Δ* strain with a decrease of 14% and 47% after 30 and 60 min, respectively. However, no difference could be observed for Sur7p, another marker of the MCC, or Pma1p, the main marker of the microdomain containing Pma1p (MCP) (Fig. 4A). This result confirms the role of Pmp3p in the control of the stability of some transporters.

The difference in the stability of Can1p between the wild-type and the *pmp3Δ* strains is moderate but reproducible. To confirm this finding, we observed the internalization of Can1p–GFP with confocal microscopy after the addition of arginine (Fig. 4B). In the wild type, Can1p–GFP was first detected exclusively at the plasma membrane in MCC at time 0. After 30 and 60 min of incubation with arginine, fluorescent foci, most probably corresponding to endosomes, were detected in the cell. After 120 min, fluorescence was observable inside the vacuole corresponding to multivesicular

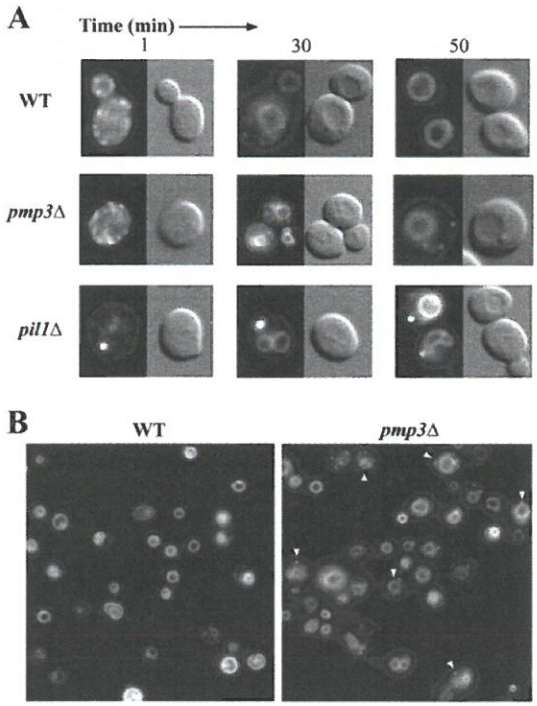

Fig. 3. FM4-64 uptake in the WT, *pmp3Δ* and *pil1Δ* strains. (A) Cells were labeled with FM4-64 on ice and excess dye was removed by washing with ice-cold YD medium, then the cells were resuspended in YD medium and incubated at 30°C for 1, 30 or 50 min. Next, endocytosis was stopped by transferring the cells to ice and adding 10 mM NaN_3 and 10 mM NaF. The cells were then observed with fluorescence microscopy (images on the left). Differential interference contrast images are shown on the right. (B) Examples of the foci seen in the *pmp3Δ* strain are indicated with arrowheads. WT, wild type.

Journal of Cell Science (2015) 128, 3646-3659 doi:10.1242/jcs.173211

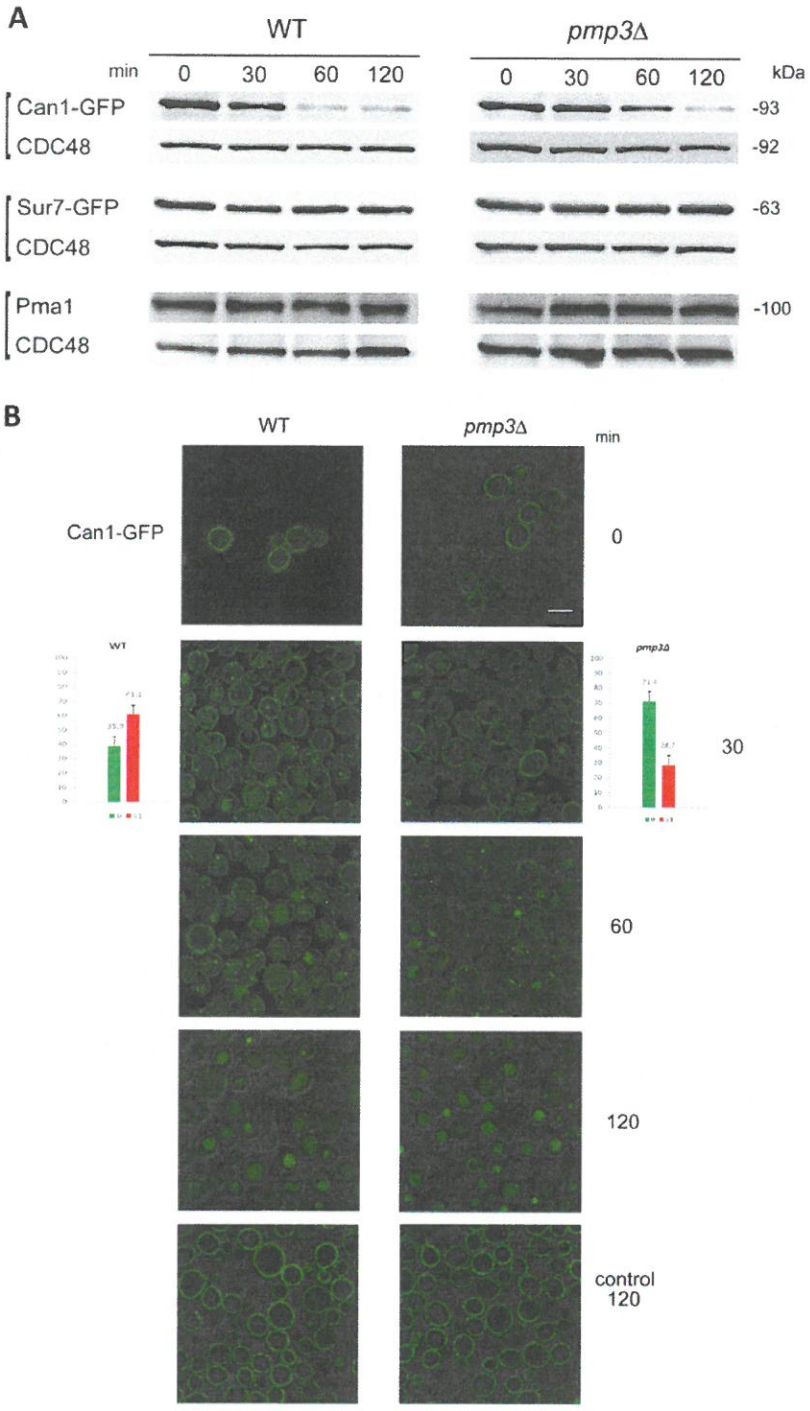

Fig. 4. Can1p turnover is reduced in the *pmp3*Δ strain. (A) Can1p–GFP, Sur7p–GFP and Pma1p stability was determined in wild-type (WT) and *pmp3*Δ strains. Protein biosynthesis was inhibited by adding cycloheximide, and the degradation rate of the indicated proteins was assessed by immunoblotting at different time points: 0, 30, 60 and 120 min. An antibody against GFP was used to detect Can1p–GFP and Sur7p–GFP. An antibody against Pma1 was used to detect Pma1p. An antibody against Cdc48p was used as a control. This figure shows one representative experiment out of three repeats. (B) Can1–GFP internalization in WT and *pmp3*Δ cells was monitored at times 0, 30, 60 and 120 min after addition of 5 mM arginine. The control culture was left untreated and observed after 120 min (bottom). Scale bar: 5 µm. Quantification was performed by analyzing more than 600 cells per condition. Graphs adjacent to the pictures represent the percentages of internalized Can1–GFP in WT and *pmp3*Δ cells. In the legend, '0' represents the percentage of cells without internal foci, whereas '≥1' represents the percentage of cells containing one or more fluorescent foci.

body (MVB)-derived internal vesicles containing Can1p–GFP. In the *pmp3*Δ strain, the same sequence was observed, although substantially delayed (Fig. 4B). For example, 29% of *pmp3*Δ cells contained internal foci compared to 60% in the wild type. After 60 min, wild-type cells contained more foci than the *pmp3*Δ cells. Moreover, 21% of the wild-type cells showed clear and exclusive vacuolar localization (without foci in the cell) compared to 11% in the *pmp3*Δ strain. After 120 min, foci were still visible in the *pmp3*Δ strain, whereas they were almost absent in the wild-type strain. This experiment confirms that Can1p–GFP internalization is delayed in the absence of Pmp3p.

Ergosterol organization is affected in a *pmp3*Δ strain

The increase in eisosome patches, as well as the decrease in the abundance of specific plasma membrane transporters, led us to analyze the plasma membrane organization of *pmp3*Δ cells. We could not show any differences in the behavior of MCP compared to the wild type (data not shown). We then analyzed the ergosterol pool

Journal of Cell Science (2015) 128, 3646-3659 doi:10.1242/jcs.173211

in the cells using filipin. We used an *erg6*Δ mutant as a control, in which the staining at the plasma membrane was drastically reduced. Interestingly, we observed that the staining of *pmp3*Δ cells was less homogenous and more punctuate at the periphery of the cells compared to that in the wild-type cells (supplementary material Fig. S3). This suggests that ergosterol organization is modified in *pmp3*Δ mutants.

*pmp3*Δ growth is modulated by sphingolipid metabolism

One explanation for the change in Pil1p regulation in *pmp3*Δ is because of an increase in LCB. We thus analyzed how *pmp3*Δ growth phenotypes could be modified by deleting genes involved in sphingolipid metabolism. In addition to the aforementioned phenotypes, we discovered that the deletion of *PMP3* confers resistance to Rhodamine 6G (Fig. 5). The toxicity of this fluorescent drug comes from its cationic and lipophilic properties, which allow it to bind to mitochondria of living cells (Johnson et al., 1981; Mottram et al., 2012) where it inhibits the F-ATPase (Wieker et al., 1987). We tested the modulation of the *pmp3*Δ growth defect on hygromycin B, NaCl and Rhodamine 6G. All of the genes used in this screening and their effect on the growth rate of *pmp3*Δ are summarized in supplementary material Table S2. The only gene deletions that modified the hygromycin B growth defect of *pmp3*Δ are involved in the addition of mannose to inositol-phosphoceramide (*SUR1*, *CSG2*) (Fig. 5) (Zhao et al., 1994; Beeler et al., 1997), or the second inositol group to mannose-inositol-phosphoceramide [MIPC] (*IPT1*, *SKN1*) (Dickson et al., 1997; Thevissen et al., 2005), or in the recycling of sphingolipids from the vacuole (*NCR1*) (Malathi et al., 2004) (Fig. 6). No strong cumulative effect could be observed for the phenotype on Rhodamine 6G. It is interesting to note that most sphingolipid-synthesis mutants have a slight resistance to Rhodamine 6G. The sensitivity to NaCl of *pmp3*Δ can be modified in both directions. The deletion of genes involved in $M(IP)_2C$ synthesis (*sur1*Δ, *csg2*Δ, *gda1*Δ, *ipt1*Δ, *skn1*Δ, *tsc3*Δ and *ncr1*Δ) improves the growth of *pmp3*Δ, whereas the deletion of *ISC1* (*isc1*Δ), the gene responsible for mannose-diinositol-phosphoceramide (M(IP)2C) catabolism, worsens it.

No cumulative effect on the growth phenotype of *pmp3*Δ grown on hygromycin B and NaCl was observed when the entire SNA family was deleted (result not shown). Owing to the fact that the deletion of *NCR1* is the only one that improves the growth of *pmp3*Δ on hygromycin B, we analyzed the effect of the deletion of the other *SNA* genes in that genomic background. We showed that *SNA2*, *SNA3* and *SNA4* share some similar functions, as deletion of the whole family is required to counter the effect of *ncr1*Δ grown on hygromycin B or NaCl (Fig. 6B). *SNA3*, like *PMP3*, improves the resistance to Rhodamine 6G when deleted. Interestingly, the absence of *PMP3* is the trigger for a growth defect on amphotericin B compared to the wild type, as the triple deletion mutant *sna2*Δ *sna3*Δ *sna4*Δ grows as well as the wild type (Fig. 6C). However, the additional *SNA* deletions worsen the growth of *pmp3*Δ. This suggests that there is a two-step function of the *SNA* family, starting with Pmp3p, which is then continued by the three other Sna proteins.

Pmp3p is less abundant in a chloroform–methanol extraction from a strain lacking sphingolipids

Because *pmp3*Δ growth phenotypes are modulated by the deletion of genes involved in sphingolipid metabolism, we wanted to estimate the expression level of Pmp3p in the absence of sphingolipids. We used an *lcb1*Δ *SLC1-1* strain that lacks serine-palmitoyl-transferase activity. The *lcb1*Δ strain is not viable. However, the *lcb1*Δ *SLC1-1* strain is viable because the *SLC1-1* allele of the 1-acyl-sn-glycerol-3-phosphate acyltransferase allows the transfer of 26-carbon (C-26) alkyl chains onto glycerol, mimicking sphingolipids (Nagiec et al., 1993). If PHS, a complex sphingolipid precursor, is added to the medium, the cell uses it to synthesize the complex sphingolipids (Dickson et al., 1990). The growth rate of this strain varies strongly, dependent upon the presence of PHS, therefore we compared the protein expression in stationary phase (OD_{600}=6.2 and 3.2, with and without additional PHS in the medium, respectively). When no PHS was added to the medium, by using chloroform–methanol extraction of total membranes, we extracted less Pmp3p (supplementary material Fig. S4).

Pmp3p binds to phosphorylated phosphoinositides, phosphatidic acid and sphingomyelin

The Pmp3p expression level is sphingolipid dependent, and phenotypic analyses of the *pmp3*Δ strain indicated that Pmp3p function is linked to sphingolipids and/or ergosterol metabolism. Because the sterol and sphingolipid pathways are tightly linked and regulated, it is important to discriminate whether a change in one is not just a side effect of a change in the other. Therefore, we tested whether Pmp3p could bind directly to sphingolipids or to ergosterol by using lipid strips. We solubilized purified plasma membranes prepared from an HA-tagged *PMP3* strain. Because sphingolipids from yeast are not commercially available, we used sphingomyelin as a representative sphingolipid for the binding test. The strip-blot showed a specific affinity for sphingomyelin and phosphatidic acid, but not for ergosterol (Fig. 7A). HA–Pmp3p also bound, but to a lesser extent, to phosphatidylcholine and phosphatidylethanolamine. As phosphatidylcholine and sphingomyelin share the same phosphocholine headgroup but have different binding affinities for Pmp3p, we can conclude that the lipid binding requires at least the ceramide portions, and possibly both the ceramide moiety and the headgroup. This result shows clearly that Pmp3p binds sphingomyelin rather than ergosterol. The affinity to phosphatidic acid, probably owing to the strong negative charge of the phosphate group, was at least tenfold higher than for sphingomyelin. The affinity of HA–Pmp3p for this negatively charged lipid led us to analyze the binding affinity for phosphoinositides. The affinity for HA–Pmp3p seemed to be stronger for PI(3)*P* and PI(3,5)P_2 than phosphatidic acid (Fig. 7B).

Sna2p and Sna4p localization is related to PI(3,5)P_2

Considering the affinity of HA–Pmp3p for phosphoinositides, the genetic interaction of *PMP3* with NCR1 (located at the vacuole), the localization of the other Sna proteins in the endosomes and vacuoles, and the increased sensitivity of *pmp3*Δ to drugs targeting the vacuole membrane (Rhodamine 6G and the toxic amyloid structure M8), we questioned whether Pmp3p, as well as vacuolar Sna2p and Sna4p, colocalize with phosphoinositide kinases and phosphatases. Because Pmp3p is a very small protein, virtually no tag leaves the protein totally functional, except for the HA–Pmp3p construct used above (results not shown). The consequence is that a fusion protein of GFP with PMP3 cannot be used. We therefore monitored the behavior of GFP-tagged Sna2p and Sna4p. Previous studies in our laboratory that have focused on the targeting sequences of these proteins have shown that the addition of GFP or dsRed does not change the localization of the proteins (Pokrzywa et al., 2009; Renard et al., 2010). The results showed that, in addition to the known vacuolar localization of Sna2p and Sna4p, they are both concentrated in a 'vacuolar dot' (Fig. 8A,B). This vacuolar dot has previously been

Journal of Cell Science (2015) 128, 3646-3659 doi:10.1242/jcs.173211

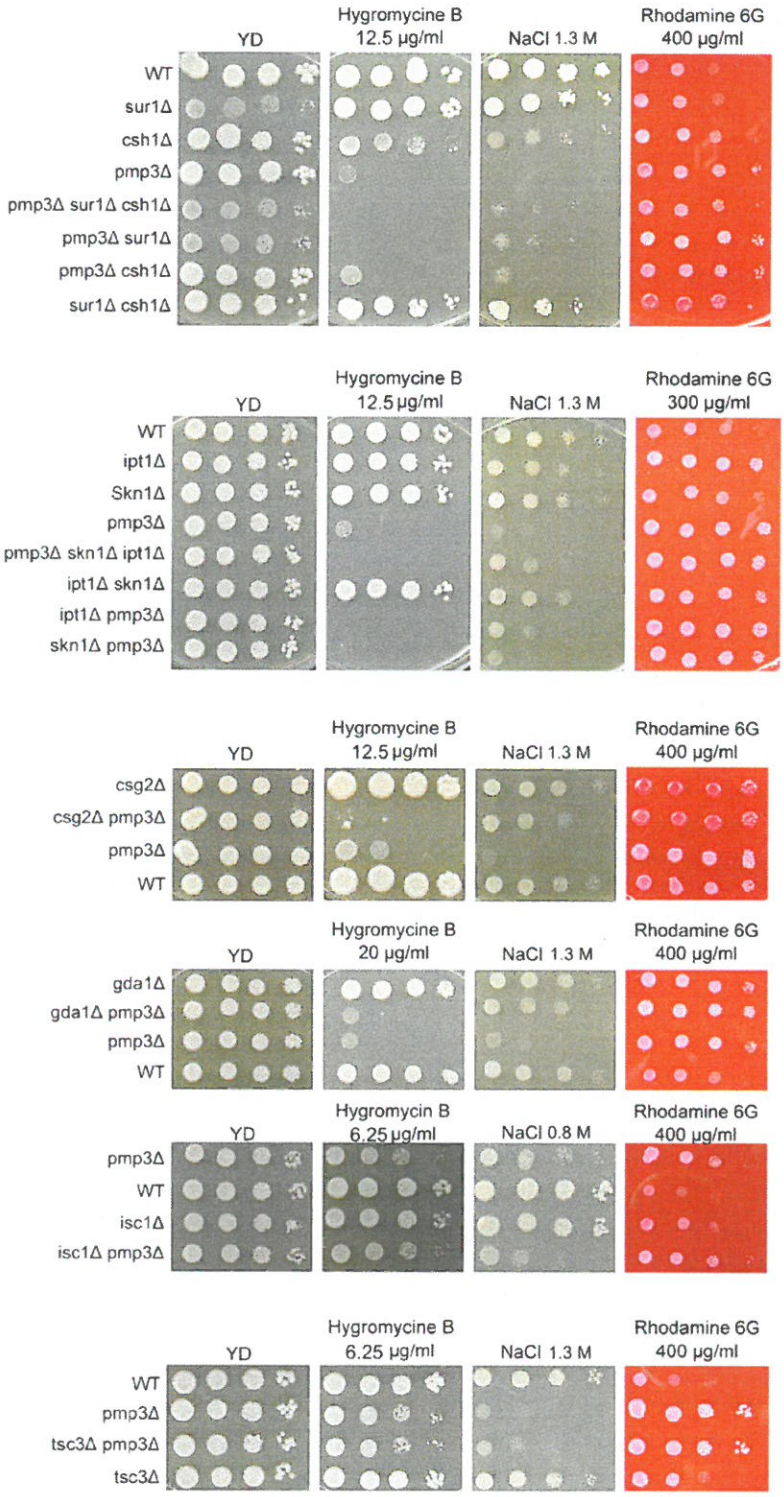

Fig. 5. The growth phenotype of *pmp3Δ* on hygromycin B and NaCl can be modulated by additional deletion of genes involved in sphingolipid metabolism. Serial tenfold dilutions of overnight saturated cultures of the indicated BY4742 strains were washed in milliQ water and dropped onto YD media that had been supplemented or not with hygromycin B, NaCl or Rhodamine 6G.

observed for Atg18–GFP (Strømhaug et al., 2004) and Fig4–GFP (Rudge et al., 2004), the latter of which is known to be in a complex with Vac14p and Fab1p (Alghamdi et al., 2013). We show here that Atg18p, Vac14p and Fab1p are also localized within this vacuolar dot and colocalize with Sna4–dsRed. Because Sna2p and Sna4p colocalize with the PI(3,5)P_2 machinery, we wondered whether their localization is PI(3,5)P_2-dependent. We show that the 'vacuolar dot' of Sna2–GFP and Sna4–GFP is lacking in a *vac14Δ* and *fab1Δ* strain (Fig. 8B). This is not the case for, at least, Sna4–GFP when *ATG18* is deleted.

Journal of Cell Science (2015) 128, 3646-3659 doi:10.1242/jcs.173211

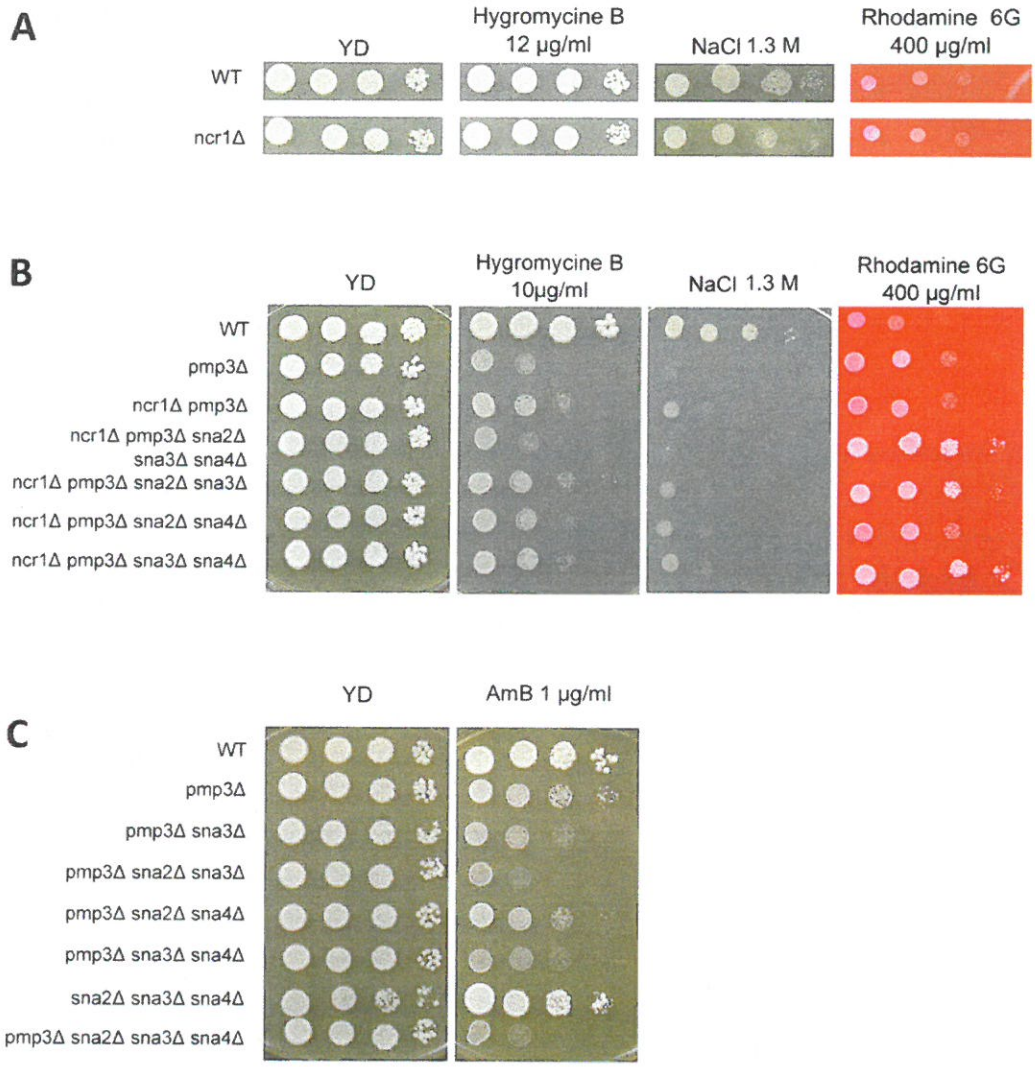

Fig. 6. The growth advantage on NaCl and hygromycin B procured by deletion of *NCR1* in a *pmp3*Δ background can be disabled by deleting the complete Sna family. Serial tenfold dilutions of overnight saturated cultures were washed in milliQ water and dropped onto YD medium that had been supplemented or not with 10 or 12 µg/ml hygromycin B, 1.3 M NaCl, 400 µg/ml Rhodamine 6G (A,B) or 1 µg/ml amphotericin B (C). A *ncr1*Δ strain had no growth advantage compared to the wild type on hygromycin B, NaCl or Rhodamine 6G (A), but deletion of *NCR1* improved the growth phenotype of *pmp3*Δ strains (B). Additional deletion of Sna genes increased the growth delays of *pmp3*Δ strains (B,C), and simultaneous deletion of *SNA2*, *SNA3* and *SNA4* is required to suppress the growth advantage conferred by deletion of *NCR1* in *pmp3*Δ strains.

DISCUSSION

In this study we have shown that the absence of Pmp3p modifies the plasma membrane proteome by decreasing the abundance of some intrinsic plasma membrane transporters and by recruiting more proteins that are involved in endocytosis. These data are correlated with the modification of the phosphorylation status of Pil1p and the modified organization of the eisosomes. These data most probably reflect a modification of lipid organization in the plasma membrane, as suggested by the numerous genetic interactions observed between *PMP3* and genes involved in sphingolipids metabolism, by the sensitivity of the *pmp3*Δ strain to amphotericin B, and by the binding of Pmp3p to sphingomyelin and phosphorylated phosphoinositides. We have tried to determine the relative amount of sphingolipids in the plasma membranes of our strains by taking a lipidomic approach. No difference was observed between wild type and *pmp3*Δ when the measurement was performed on total cell lysates (data not shown). However, we were unable to measure the lipid composition in the plasma membrane itself owing to very high variability of the data. This could be due to contamination of our plasma membrane extracts by lipid droplets. However, the pool and/or the distribution of ergosterol must be modified considering the sensitivity to amphotericin B and the filipin staining in *pmp3*Δ compared to the wild type. This hypothesis is supported by a previous study showing that the double deletion *pmp3*Δ *ncr1*Δ strain has a growth defect under anaerobic conditions compared to the single deletion mutants and the wild type (Munkacsi et al., 2011). Under anaerobic growth conditions, different yeasts cannot synthesize sterols, and these must be imported from the medium. As a number of phenotypic interactions were observed between *NCR1* and the Sna family, we analyzed the growth of several *ncr1*Δ *sna*Δ strains.

Journal of Cell Science (2015) 128, 3646-3659 doi:10.1242/jcs.173211

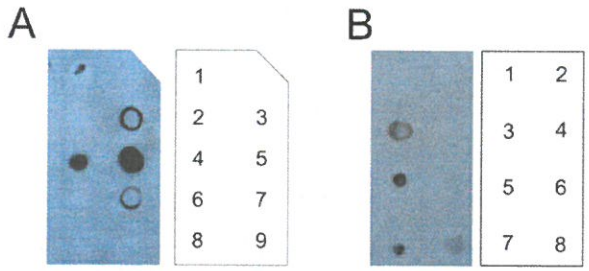

1: phosphatidylcholine100 nmol
2: ergosterol 100 nmol
3: phosphatidylethanolamine 100 nmol
4: sphingomyelin 100 nmol
5: phosphatidic acid 100 nmol
6: sphingomyelin 10 nmol
7: phosphatidic acid 10 nmol
8: sphingomyelin 1 nmol
9: phosphatidic acid 1 nmol

(all at 100 nmol)
1: ergosterol
2: PI
3: phosphatidic acid
4: sphingomyelin
5: PI(3)P
6: PI(4)P
7: PI(3,5)P_2
8: PI(4,5)P_2

Fig. 7. HA–Pmp3p preferentially binds to phosphatidic acid, PI(3)*P* and PI(3,5)P_2, and to a lesser extent PI(3,5)P_2 and sphingomyelin but not ergosterol. Nitrocellulose membranes were spotted with chloroform-solubilized lipids (100 nmol or less) and incubated for 3 h with 3 ml of purified and zwittergent-3-14-solubilized plasma membranes of the BY4742+pRS316 HA–Pmp3 strain (0.5 µg proteins/ml). Detection was performed using antibodies against HA. A 150-s exposure of a phospholipid, ergosterol and sphingomyelin strip showed a preferential binding of HA–Pmp3p for phosphatidic acid and, to a tenfold lesser extent, sphingomyelin (A). A 15-s exposure of a sphingomyelin and phosphoinositide strip revealed the more intense affinity for phosphoinositides than sphingomyelin (B). The experiment was repeated three times.

Unfortunately, we were unable to reproduce the results of Muncaksi et al., even when the entire Sna family was deleted (data not shown). Finally, we were unable to show that HA–Pmp3p binds to ergosterol *in vitro*, which suggests that modification of the abundance of ergosterol could be a side effect of other changes in lipid organization of the plasma membrane. HA–Pmp3p binds to sphingomyelin, and *PMP3* has a PHS-dependent expression level in *lcb1Δ SLC1*, as well as several genetic interactions with genes involved in sphingolipid metabolism. The above mentioned phenotypes could thus be side effects of altered sphingolipid regulation.

The effects of *PMP3* deletion can be seen on Pil1p behavior, such as reduced phosphorylation of Pil1p and formation of fewer eisosomes per cell in *pmp3Δ*. There might be several reasons for Pil1p deregulation: an excess of LCBs, an excess of Nce102p abundance, a drop in the abundance of the Pkh kinases responsible for Pil1p phosphorylation, or a reduction of in Mss4p – the phosphatidylinositol-4-phosphate 5-kinase. Because deletion of genes in the sphingolipid pathway modulates the growth phenotype of *pmp3Δ*, it is likely that there is an excess of sphingolipid precursors, the LCBs, in *pmp3Δ* strains. However, the additional deletion of the LCB-dependent Pkh regulator *NCE102* in a *pmp3Δ* strain rescues, only to a small degree, the growth defect on hygromycin B (data not shown). Pil1p deregulation in *pmp3Δ* is thus probably not the result of an excess of LCB or Nce102p. As the Pkh kinases have several effectors, it does not seem possible to have a lack in these proteins. Their absence or decrease in abundance should have a drastic effect on yeast growth. The final hypothesis is a change in phosphoinositide abundance. This hypothesis is possible because HA–Pmp3p binds strongly to PI(3)*P* and PI(3,5)P_2, and to a lesser extent to PI(4,5)P_2. Moreover, Sna4–dsRed colocalizes with Atg18–GFP, Vac14–GFP and Fab1–GFP. Sna2–GFP and Sna4–GFP localize to a typical vacuolar dot in a PI(3,5)P_2-dependent manner. These data strongly suggest that Sna proteins interact with phosphoinositides. This interaction could in turn affect sphingolipid organization in the plasma membrane and Pil1p recruitment. As a side effect, endocytosis could be slightly modified by a change in microdomain organization of the plasma membrane, as shown by filipin staining. Interestingly, the *SNA3* gene is in tandem with *INO1* and is regulated in an inositol-mediated manner (Shetty et al., 2013), which is in accordance with a lipid regulatory process.

Our results are in accordance with the epistatic microarray analysis of the plasma membrane performed previously by Aguilar et al. (2010). That study revealed that amongst the most positive genetic interactions of *PMP3* are the genes *SUR1*, *ERG5* and *IPT1*. *ERG5* is a C-22 sterol desaturase that is involved in ergosterol biosynthesis (Skaggs et al., 1996). The most negative genetic interactions of *PMP3* are with *FAB1*, *PIL1* and *SLI1*. The latter is an N-acetyltransferase, which confers resistance to the sphingolipid biosynthesis inhibitor myriocin by converting it into N-acetyl-myriocin (Momoi et al., 2004). The genes that had an epistatic microarray profile that was most correlated to that of *PMP3* are *SLA1*, *RVS161* and *RVS167*. These three genes are involved in endocytosis. Deleting *PIL1* affects the scission efficiency and the frequency of the formation of endocytic sites carrying Rvs161– and Rvs167–GFP (Murphy et al., 2011). It is important to note that the name of *SUR1*, bearing the most positive genetic interaction with *PMP3*, is 'Suppressor of Rvs161 and Rvs167 mutations' (Desfarges et al., 1993).

We have shown that the deletions of *SNA2*, *SNA3* and *SNA4* have a cumulative effect on the growth of *pmp3Δ* on amphotericin B, and that the deletion of the whole Sna family is required to cancel the growth advantage provided by the deletion of *NCR1* in a *pmp3Δ* background. This result shows that the *SNA* genes share a common function. Ncr1p seems to be responsible for the recycling of MIPC from the vacuole (Malathi et al., 2004). We know from our drop tests that at least one protein among Sna2p, Sna3p and Sna4p is required to allow the function of *NCR1* (e.g. sphingolipid recycling) to take place. Even though these three Sna proteins are localized at/in the vacuole and share a similar function, they have specificities regarding the growth phenotypes. The deletion of *SNA3* is the only gene that increases the resistance of *pmp3Δ* to Rhodamine 6G, and *SNA4* deletion has no effect on growth on amphotericin B.

Considering that Pmp3p binds to phosphoinositides, that Sna2p and Sna4p localize in a phosphoinositide-dependent manner and colocalize with PI(3,5)P_2, that the four Sna proteins share a similar function and that *PMP3* deletion influences Pil1p behavior, and thus plasma membrane organization, we suggest that Pmp3p is involved in a phosphoinositide regulatory system between the plasma membrane and the vacuole. Because Pmp3p also binds to sphingomyelin and has a sphingolipid-dependent expression, and because *PMP3* has many genetic interactions with genes involved in sphingolipid synthesis, *PMP3* might be part of a regulatory mechanism between phosphoinositides and sphingolipids.

MATERIALS AND METHODS

The *S. cerevisiae* strains used are listed in supplementary material Table S3.

Cells were transformed using the LiOAc method, developed by Schiestl et al. (Schiestl and Gietz, 1989). The following solutions were used: Li-TE, 100 mM LiOAc in acetic acid pH 7.5, 1/10 Tris EDTA (10 mM Na_2EDTA, 100 mM Tris-HCl pH 7.7]; polyethylene glycol (PEG), 35 g PEG 400 in a total volume of 50 ml of 1× Tris EDTA; salmon sperm DNA in water boiled for 10 min at 100°C, then stored at −20°C.

Journal of Cell Science (2015) 128, 3646-3659 doi:10.1242/jcs.173211

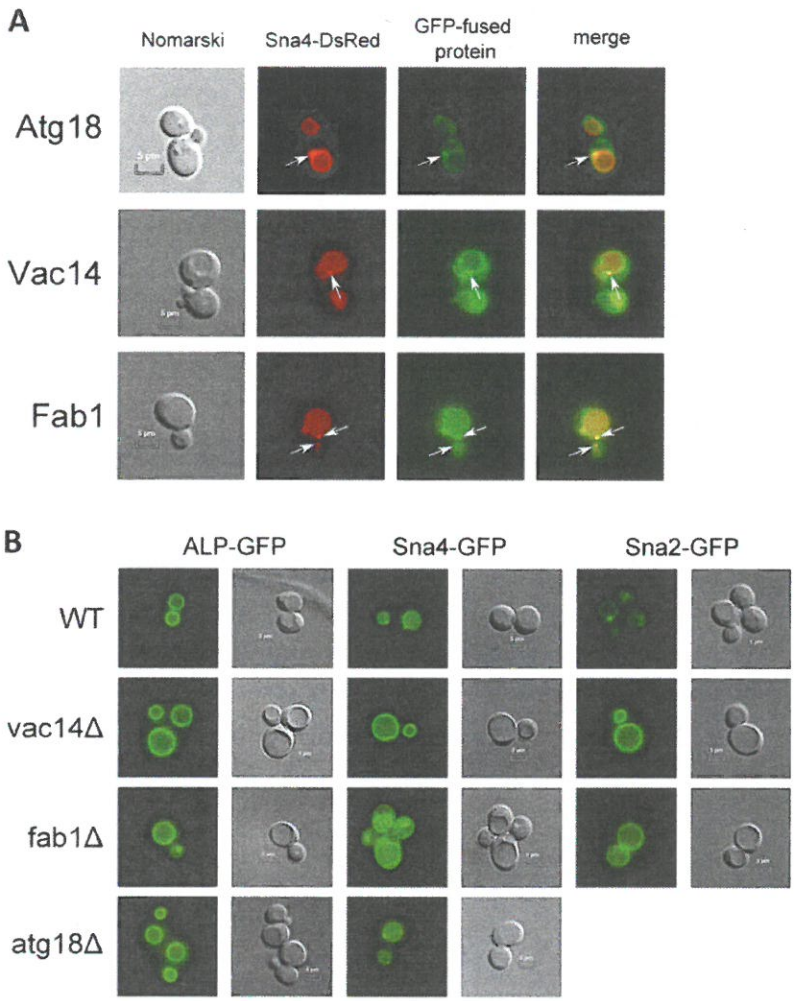

Fig. 8. Sna4–GFP and Sna2–GFP localization is PI(3,5)P_2-dependent. (A) Atg18–GFP, Vac14–GFP and Fab1–GFP colocalized with Sna4–dsRed in a 'vacuolar dot' (arrows). Images represent the mid-section of cells taken with an epifluorescence microscope. (B) The formation of the vacuolar dot of Sna4–GFP and Sna2–GFP was PI(3,5)P_2-dependent. GFP, green. ALP-GFP, GFP-tagged alkaline phosphatase.

The 3′ 6HA-tagged genes were transformed through a PCR cassette from the plasmid pYM15 containing the 6HA tag and a *HIS3MX6* prototrophic marker, from the PCR Toolbox of Euroscarf (Janke et al., 2004). The strains were grown at 28°C in rich yeast dextrose (YD) medium [2% (w/v) yeast extract KAT and 2% (w/v) glucose], yeast peptone dextrose (YPD) medium [1% (w/v) bacto yeast extract, 2% (w/v) glucose, 2% (w/v) peptone] or drop-out medium [0.7% (w/v) bacto yeast nitrogen base without amino acids, 2% (w/v) glucose, 40 µg/ml adenine hemisulfate salt and required amino-acids: 20 µg/ml L-arginine (HCl), L-histidine, L-methionine, uracil, 30 µg/ml L-lysine mono-HCl and L-tyrosine, 40 µg/ml L-tryptophan, 50 µg/ml L-phenylalanine, 60 µg/ml L-leucine, 100 µg/ml L-aspartic acid and L-glutamic acid, 150 µg/ml L-valine, 200 µg/ml L-threonine and 375 µg/ml L-serine]. Solid media also contained 2% agar (Sigma). Hygromycin B (Sigma-Aldrich), Rhodamine 6G (Merck), amphotericin B (Sigma-Aldrich), PHS (TCI) from stock solution (10 mg/ml in ethanol) or ethanol were added after autoclave before spreading onto Petri dishes as indicated. Yeast samples for real-time PCR analysis (2 ml OD_{600}=0.25) were centrifuged, and the cell pellets were immediately frozen in liquid nitrogen and stored at −80°C until RNA extraction. Phosphatidylcholine 17:0–14:1 (LM-1004), phosphatidylethanolamine 17:0–14:1 (LM-1104), phosphatidylinositol 17:0–14:1 (LM-1504), phosphatidylserine 17:0–14:1 (LM-1304), C17:0 ceramide (860517) and C8-glucosyl(β)ceramide (860540) were used as internal lipid standards, and were purchased from Avanti Polar Lipids (Alabaster, AL). Cholesterol was used as a sterol standard and was purchased from Fluka (Sigma-Aldrich, Steinheim, Germany). Pyridine (ReagentPlus®) and methylamine solution (33% in absolute ethanol) were from Sigma-Aldrich (Steinheim, Germany). HPLC-grade chloroform was purchased from Acros (Geel, Belgium), LC-MS-grade methanol and LC-MS-grade ammonium acetate were from Fluka (Sigma-Aldrich, Steinheim, Germany). LC-MS-grade water was purchased from Fisher Scientific (Loughborough, UK). Strip-blots were performed with phosphatidic acid, phosphatidylinositol (L-α-phosphatidylinositol ammonium salt, from bovine liver, Sigma-Aldrich), phosphatidylserine, phosphatidylethanolamine (L-α-phosphatidylethanolamine Type III-A, Sigma-Aldrich), PHS (TCI), ergosterol (Fluka)and sphingomyelin (from egg yolk, 99%, Sigma-Aldrich).

Total RNA extraction

Frozen cells were mechanically disrupted using a cell homogenizer (Precellys). Total RNA was extracted using the RNeasy minikit (Quiagen) with the additional RNase-free DNase set (Qiagen). The extracted RNA was quantified using a nanodrop 1000 spectrophotometer (Nanodrop Technologies, Wilmington, DE).

Quantitative RT-PCR

Oligonucleotides for real-time PCR (supplementary material Table S4) were designed using the Mfold server, Primer3 plus (http://www.bioinformatics.nl/cgi-bin/primer3plus/primer3plus.cgi), Oligoanalyzer (http://eu.idtdna.com/analyzer/applications/oligoanalyzer/) and primer-BLAST.

13.5 µl of RNA was mixed with 2 µl degenerated poly-T 20 µM, heated at 70°C for 5 min, then cooled directly in ice to avoid re-folding. The sample was then complemented with 5 µl M-MLV 5× reaction buffer (Promega),

Journal of Cell Science (2015) 128, 3646-3659 doi:10.1242/jcs.173211

1 µl M-MLV reverse transcriptase (Promega), 1 µl recombinant RNAsin ribonuclease inhibitor and 2.5 µl dNTPs 10 mM. The mix was then incubated at 37°C for 1 h.

The cDNA levels were analyzed using the Step One Plus Real-Time PCR systems (Applied Biosystems). Each sample was tested in triplicate in a 96-well plate. The reaction mix (20 µl final volume) comprised 10 µl SYBR green mix (Eurogentec), 5 µl cDNA diluted from 1:1 to 1:10,000 and 5 µl of the primer set (see supplementary material Table S4 for final concentrations). A blank (no cDNA) sample was also incorporated for each assay (in triplicate). The thermocycling program comprised of one hold at 95°C for 10 min, followed by 40 cycles of 15 s at 95°C and 1 min at 60°C.

After completion of these cycles, melting-curve data were then collected to verify PCR specificity, contamination and the absence of primer dimers.

The PCR efficiency of each primer pair was evaluated using the dilution series method with a mix of sample cDNAs as the template. Briefly, it was determined from standard curves using the formula $10^{(-1/\text{slope})}$. For the calculations, the base of the exponential amplification function was used (e.g. 1.97 means 97% amplification efficiency). Relative expression levels were determined with efficiency correction (Pfaffl, 2001).

Total protein extracts

Cell cultures (5 ml) at the required optical density were centrifuged. Pellets were washed once with 1 ml water, then resuspended in 200 µl of lysis buffer [25 mM Tris-HCl pH 7.5, 5 mM Na_2EDTA, 1 mM PMSF, protease inhibitor cocktails (2 µg/ml each of leupeptin, aprotinin, antipain, pepstatin and chymostatin)] with 200 µl of glass beads 0.5–0.7 mm in diameter (VWR). Samples were vortexed eight times for 30 s each with a 15-s pause on ice between each vortex. Samples were centrifuged for 1 min at 2500 ***g***, and supernatants were collected into new tubes, put into liquid nitrogen and kept at −80°C.

Plasma membrane purifications

All steps were performed at 4°C. Four liters of cells were harvested at OD_{600}=3 by centrifuging at 5000 rpm for 5 min (ILA.9100, Beckman), washed with 0.5 l of cold distilled water, and resuspended in 15 ml of cold homogenization medium (250 mM sorbitol, 50 mM imidazole, 1 mM $MgCl_2$, pH 7.5) containing a protease inhibitor mix [1 mM phenylmethylsulfonyl fluoride (PMSF) and 2 µg/ml each of leupeptin, aprotinin, antipain, pepstatin and chymostatin] per 10 g of cells, and the suspension was poured into a 75-ml homogenizer glass flask. Glass beads were added at a ratio of 15 g per 10 g of cells, and the suspension was homogenized in a Braun MSK homogenizer (Helsungen, Germany) for 3 min at full speed with cooling. Cell debris and unbroken cells were eliminated by two 5-min centrifugations at 3000 rpm and one 5-min centrifugation at 6000 rpm (JA-30.50Ti, Beckman). The supernatant was then centrifuged for 45 min at 14,000 rpm (JA-30.50Ti, Beckman) to pellet crude membranes (C15/40), which were resuspended in 5 ml of suspension medium (10 mM imidazole, 2 mM $MgCl_2$, pH 7.5, containing the protease inhibitor mix) per 10 g of cells. The suspension containing crude membranes was homogenized and brought to pH 4.8 with 1 M acetic acid, and protein aggregates were removed by centrifuging at 8000 rpm for 2 min (JA-30.50Ti, Beckman). The supernatant was rapidly neutralized (pH 7.5) with 1 N NaOH and centrifuged for 30 min at 42,000 rpm (70TI, Optima-Beckman). Depending on the use, the protein pellet was either resuspended in suspension medium for western blotting or immune precipitation analysis and stored at −80°C, or resuspended in 50 mM triethyl ammonium bicarbonate (TEAB), pH 8.0, and stored at 20°C until use for mass spectrometry analysis.

Membrane stripping before iTraq

The membranes were incubated in 0.1 M sodium carbonate, 50 mM TEAB, pH 11.5, for 30 min on ice, then centrifuged at 48,000 rpm for 30 min (TLA55, Optima-Beckman) to pellet the stripped membranes, which were resuspended in 50 mM TEAB.

Bicinchoninic assay

Five microliters of protein was diluted in 45 µl of milliQ water. Standards were made with 5 µl of the same buffer as proteins, bovine serum albumin (2 mg/ml) in increasing doses from 0 to 10 µl and milliQ water to reach a final volume of 50 µl. $CuSO_4.7H_2O$ 4% (w/v) was diluted at a 1/50 ratio in bicinchoninic acid. One milliliter of this mix was added to each sample, mixed, and incubated for 30 min at 37°C. Once samples had cooled down, absorbance was read at 562 nm.

SDS-PAGE and immunoblotting

Protein samples were mixed with an equal volume of sample buffer [100 mM Tris-HCl, pH 6.8, 4 mM Na_2EDTA, 4% SDS, 20% glycerol, 0.002% bromophenol blue (and 9 M urea for Pdr5-6HA samples)] containing 1% dithiothreitol and incubated at 37°C (56°C for Pdr5–6HA samples) for 10 min, then the proteins were separated by SDS-PAGE and transferred to a PVDF membrane (Millipore, Billerica, MA) using a semi-dry transfer system (Bio-Rad, Hercules, CA) in 50 mM Tris, 40 mM glycine, 0.0375% SDS and 20% methanol. For the analysis of HA–Pmp3p, separated proteins were transferred through wet transfer (50 V, 23 min) in Tris 0.3% w/v, glycine 1.4% w/v, methanol 20% v/v. The blot was saturated overnight at 4°C using 5% low-fat dried milk in Tris-buffered saline (TBS; 50 mM Tris, 150 mM NaCl, pH 7.6) containing 0.5% Tween-20; the membranes were then incubated at room temperature for 1.5 h with anti-HA rat antibodies, anti-Pma1p rabbit antibodies or anti-Pil1p antibodies (dilution 1:10,000) diluted in TBS, 0.5% Tween-20 containing 0.5% low-fat milk. After three washes with TBS containing 0.1% Tween-20, the blot was incubated at room temperature for 45 min with horseradish-peroxidase-coupled anti-rat (dilution 1:10,000, Roche) or anti-rabbit IgG (dilution 1:10,000, Chemicon International, Temecula, CA) antibodies, followed by chemiluminescence detection (Roche Diagnostics, Indianapolis, IN). The signals were captured and quantified using a KODAK 4000R Image Station, driven by KODAK Molecular Imaging Software version 4.0. The rabbit polyclonal antibodies directed against Pma1p were generated from highly purified plasma membrane Pma1 protein from *Schizosaccharomyces pombe*. The anti-Pil1p antibodies were kindly provided by Pablo S. Aguilar (Institut Pasteur de Montevideo, Uruguay).

Proteolipid extraction using chloroform–methanol

C15/40 samples, as concentrated as possible (10 mg/ml of proteins is optimal), were suspended in 25 volumes of a mixture of chloroform–methanol (2 :1) for 2 h at 4°C on an agitating wheel at 40 rpm. Undissolved material was removed by filtration through a Buchner funnel. The extract was washed with 0.2 volumes of water of remaining material. After centrifugation of the milky emulsion at 2000 ***g*** for 30 min, the lower organic phase was concentrated to 300 µl under reduced pressure in a speedvac at 40°C. Chloroform extracts were then transferred to 2 ml Eppendorf tubes. Former sample tubes were washed with 100 µl chloroform, which was then added to the samples. Four volumes of diethyl ether were added to the sample, and the mixture was stored for 1 h at −20°C. Precipitated proteins were collected by a 30-min centrifugation at 20,000 ***g*** at 4°C. The pellet was then resuspended in suspension buffer.

Protein digestion and iTRAQ labeling

Purified plasma membranes (20 µg of protein) were solubilized in 50 mM TEAB, 0.1% Rapigest (Waters), pH 8.0, by sonicating for 5 min in a bath sonicator (Bioruptor, Diagenode), and the proteins were reduced by incubation for 1 h at 60°C with 25 mM tris(2-carboxyethyl)phosphine and then alkylated with 0.25 M methyl-methanethiosulfonate for 10 min at room temperature in the dark. The reduced and alkylated proteins were digested for 16 h at 37°C by using sequencing-grade modified trypsin (Promega, Madison, WI) at a protease:protein ratio of 1:20, and the Rapigest detergent was lysed by incubating the protein sample in 0.5% trifluoroacetic acid (TFA) for 60 min at 37°C. After centrifugation of the sample at 54,000 rpm (TLA55, Optima-Beckman) for 45 min at 4°C, the supernatant was centrifuged for 20 min at 54,000 rpm (TLA55, Optima-Beckman), then the final supernatant was vacuum dried (Speedvac SC 200, Savant) and iTRAQ labeling performed according to the manufacturer's protocol (Applied Biosystems, Foster City, CA). The samples were labeled with tag 114 for the control, tag 115 for the 10 min sample, tag 116 for the 30 min sample and tag 117 for the 90 min sample.

Reverse-phase chromatography

Before separation, the samples were dissolved in 0.025% trifluoroacetic acid (TFA) and 5% acetonitrile (ACN), then the labeled peptides were mixed together and 12.9 µg of the mixture desalted using a C18 Pep Map 100 pre-column and subjected to reverse-phase chromatography on a C18 PepMap100 (LC Packings) analytical column for 180 min at a flow rate of 300 nl/min using a linear gradient from 8% ACN in water with 0.1% TFA to 76% ACN in water with 0.085% TFA. The eluted peptides were mixed with α-cyano-4-hydroxycinnamic acid matrix (2 mg/ml in 70% ACN, 0.1% TFA) and spotted directly onto a matrix-assisted laser desorption ionization (MALDI) target using a Probot system (LC Packings Amersham Biosciences).

Mass spectrometry analysis

The spotted plate was analyzed on an Applied Biosystems 4800 MALDI time-of-flight (TOF)/TOF Analyzer using a 200-Hz solid-state laser operating at 355 nm. Mass spectrometry spectra were obtained using a laser intensity of 3200 and 2000 laser shots per spot in the *m/z* range of 800 to 4000, whereas MS/MS spectra were obtained by automatic selection of the 12 most intense precursor ions per spot using a laser intensity of 3800 and 2100 laser shots per precursor. Collision-induced dissociation was performed with an energy of 1 kV with air as the collision gas at a pressure of 1×10^{6} Torr. Data were collected using Applied Biosystems 4000 Series Explorer™ software. LC MS/MS data were processed using ProteinPilot software and the Paragon™ search algorithm (Shilov et al., 2007) (Applied Biosystems/MDS SCIEX/4800 version 2.0). The MS/MS data were used to search the UniProtKB–Swiss-Prot database (276,256 sequences Release 54.0 of 24, July 07 from the website http://www.ebi.ac.uk/FTP/) using the 'thorough search' option and a *S. cerevisiae* taxonomy filter. The 'iTRAQ 4plex peptide labeled' sample type and a 'biological modification ID focus' were selected in the analysis method. Trypsin was selected as the digestion enzyme, with cysteine alkylation by methyl-methanethiosulfonate as a modification. The results were further processed by the Pro Group™ Algorithm to determine the minimal set of justifiable identified proteins. Proteins were annotated based on Saccharomyces Genome Database (SGD), Gene Bank and UniProt Databases.

Data were normalized using ProteinPilot. All reported data were based on 99% confidence for protein identification as determined by ProteinPilot (ProtScore≥2.0). Protein identification confidence was expressed as the 'Unused Protein Score', a measurement of the protein identification confidence taking into account peptides from spectra that have not already been 'used' by higher scoring proteins.

Quantification of relative change

To determine differences in expression of proteins between *pmp3*Δ and the control, the average ratio of the identified protein was calculated by ProteinPilot based on the weighted-average log ratios of the peptides. Differentially expressed proteins were further analyzed for significant down- or upregulation, which was calculated by ProteinPilot. A cut-off level of significance of 95% (or $P<0.05$) was chosen as a criterion for each individual experiment. Peptides that matched multiple proteins were not included in the quantification by the software. The final ratios were calculated from the average of the ratios obtained in at least two independent experiments in which the change in protein abundance was significant ($P<0.05$). In each experiment, bias correction for unequal mixing during the combination of the different labeled samples was performed. This correction is based on the assumption that most proteins do not change in expression. Thus, if samples from each experimental condition are not combined in exactly equal amounts, bias correction fixes this systematic error. The software identifies the median average protein ratio and corrects it to unity, and then applies this factor to all quantification results.

Strip-blot

Sterols were solubilized to 25 mM in chloroform. Other lipids were solubilized in chloroform to reach a final concentration of 14.286 mM. Four microliters of sterols or 7 µl of other lipids were spotted on a nitrocellulose membrane, which was then left to dry for 30 min. At this point, all the steps were performed on an agitating table at 60 rpm. The membrane was saturated overnight at 4°C in 4 ml TBS Tween-20 0.1% with 3% fatty-acid-free bovine serum albumin. The strip was then incubated for 3 h at 4°C with 3 ml of Zwittergent-3-14-solubilized plasma membranes (0.5 mg/ml proteins at 1:10 protein to detergent ratio) to which we added 330 µl TBS Tween-20 1% before incubation. The membrane was then washed three times for 10 min in 3 ml TBS Tween-20 0.1%. The lipid-coated strip was then incubated for 90 min with 4 ml TBS Tween-20 0.1%, fatty-acid-free bovine serum albumin 3% and 4 µl of anti-HA antibodies. The membrane was washed as described previously, then incubated for 45 min with 4 ml TBS Tween-20 0.1%, fatty-acid-free BSA 3% and 0.4 µl of anti-rat IgG antibodies. After a wash (as previously described), the membrane was incubated for 1 min in BM chemiluminescence blotting substrate (POD) (4 ml solution A and 40 µl solution B) (Roche). Luminescence was captured on film in a dark room for 1 min and processed by an Optimax x-ray film processor. The specificity of anti-HA antibodies has been verified. No signal was detected with extracts from wild-type untagged cells.

Filipin (sterol) fluorescence microscopy

To examine sterol distribution using filipin, 10 ml of cells grown to a density of 0.5 OD_{600} units/ml were fixed with 1 ml of 37.5% formaldehyde for 10 min at 28°C with constant shaking. Fixed cells were washed twice and resuspended in PBS. Filipin (Sigma F9765) was added to the cell suspension at a final concentration of 100 µg/ml. After incubating at 28°C in the dark with filipin, cells were spotted on agarose-coated slides and filipin fluorescence was observed on the Leica DMR epifluorescence microscope with a 100× oil immersion objective. Excitation was performed at 360 nm, and emission was captured at 470 nm.

Endocytosis assays

FM4-64 uptake was measured as described previously by Walther et al. (2006). The cells were grown to exponential phase in YD medium to an OD_{600} of 1 and centrifuged at 960 ***g*** for 1 min. All but 100 µl of the medium was removed, and 1 µl of FM4-64 (16 mM; Invitrogen) was added, then the cells were resuspended and incubated for 15 min on ice. The cells were washed twice with ice-cold medium, centrifuged at 6800 ***g*** for 1 min, resuspended in 1 ml of fresh medium, and incubated for 1, 30 or 50 min at 30°C. Incubation was stopped and 10 mM NaN_3 and 10 mM NaF were added. Fluorescence was observed with a Texas-Red filter.

Acknowledgements

The authors thank Pablo S. Aguilar (Institut Pasteur de Montevideo, Uruguay) for providing the anti-Pil1 antibody, Professor Roger Schneiter (Université de Fribourg, Fribourg, Switzerland) for the *lcb1*Δ *SLC1-1* strain, Howard Riezman and Auxi Aguilera-Romero for lipidomics analysis. We thank Michel Ghislain, Joost Holthuis, Henri-François Renard, Auxi Aguilera-Romero for critical reading of the paper.

Competing interests

The authors declare no competing or financial interests.

Author contributions

J.D.B., A.S., B.G., J.D., J.-F.H. and P.M. designed research; J.D.B., A.S., B.G., J.D., J.-F.H. and J.V. performed research; J.D.B., A.S., B.G., J.D., J.-F.H., J.V. and P.M. analyzed data; and J.D.B., J.-F.H. and P.M. wrote the paper.

Funding

This work was supported by grants from the Fonds National de la Recherche Scientifique (FNRS); and the Fédération wallonie-Bruxelles (ARC). J.D.B., A.S., B.G., J.V., J.D. and J.-F.H. are research fellows at the 'Fonds pour la Formation à la Recherche dans l'Industrie et dans l'Agriculture'.

Supplementary material

Supplementary material available online at
http://jcs.biologists.org/lookup/suppl/doi:10.1242/jcs.173211/-/DC1

References

Aguilar, P. S., Fröhlich, F., Rehman, M., Shales, M., Ulitsky, I., Olivera-Couto, A., Braberg, H., Shamir, R., Walter, P., Mann, M. et al. (2010). A plasma-membrane E-MAP reveals links of the eisosome with sphingolipid metabolism and endosomal trafficking. *Nat. Struct. Mol. Biol.* **17**, 901-908.

Alghamdi, T. A., Ho, C. Y., Mrakovic, A., Taylor, D., Mao, D. and Botelho, R. J. (2013). Vac14 protein multimerization is a prerequisite step for Fab1 protein complex assembly and function. *J. Biol. Chem.* **288**, 9363-9372.

Bari, V. K., Sharma, S., Alfatah, M., Mondal, A. K. and Ganesan, K. (2015). Plasma membrane proteolipid 3 protein modulates amphotericin B resistance through sphingolipid biosynthetic pathway. *Sci. Rep.* **5**, 9685.
Beeler, T. J., Fu, D., Rivera, J., Monaghan, E., Gable, K. and Dunn, T. M. (1997). SUR1 (CSG1/BCL21), a gene necessary for growth of Saccharomyces cerevisiae in the presence of high Ca2+ concentrations at 37°C, is required for mannosylation of inositolphosphorylceramide. *Mol. Gen. Genet.* **255**, 570-579.
Bolard, J. (1986). How do the polyene macrolide antibiotics affect the cellular membrane properties? *Biochim. Biophys. Acta* **864**, 257-304.
Carroll, S. Y., Stimpson, H. E. M., Weinberg, J., Toret, C. P., Sun, Y. and Drubin, D. G. (2012). Analysis of yeast endocytic site formation and maturation through a regulatory transition point. *Mol. Biol. Cell* **23**, 657-668.
Couthouis, J., Marchal, C., D'Angelo, F., Berthelot, K. and Cullin, C. (2010). The toxicity of an "artificial" amyloid is related to how it interacts with membranes. *Prion* **4**, 283-291.
D'Angelo, G., Vicinanza, M., Di Campli, A. and De Matteis, M. A. (2008). The multiple roles of PtdIns(4)P - not just the precursor of PtdIns(4,5)P2. *J. Cell Sci.* **121**, 1955-1963.
Dennis, V. W., Stead, N. W. and Andreoli, T. E. (1970). Molecular aspects of polyene- and sterol-dependent pore formation in thin lipid membranes. *J. Gen. Physiol.* **55**, 375-400.
Desfarges, L., Durrens, P., Juguelin, H., Cassagne, C., Bonneu, M. and Aigle, M. (1993). Yeast mutants affected in viability upon starvation have a modified phospholipid composition. *Yeast* **9**, 267-277.
Dickson, R. C., Wells, G. B., Schmidt, A. and Lester, R. L. (1990). Isolation of mutant Saccharomyces cerevisiae strains that survive without sphingolipids. *Mol. Cell. Biol.* **10**, 2176-2181.
Dickson, R. C., Nagiec, E. E., Wells, G. B., Nagiec, M. M. and Lester, R. L. (1997). Synthesis of mannose-(inositol-P)2-ceramide, the major sphingolipid in Saccharomyces cerevisiae, requires the IPT1 (YDR072c) gene. *J. Biol. Chem.* **272**, 29620-29625.
Erez, O. and Kahana, C. (2002). Deletions of SKY1 or PTK2 in the Saccharomyces cerevisiae trk1 Delta trk2 Delta mutant cells exert dual effect on ion homeostasis. *Biochem. Biophys. Res. Commun.* **295**, 1142-1149.
Faergeman, N. J., DiRusso, C. C., Elberger, A., Knudsen, J. and Black, P. N. (1997). Disruption of the Saccharomyces cerevisiae homologue to the murine fatty acid transport protein impairs uptake and growth on long-chain fatty acids. *J. Biol. Chem.* **272**, 8531-8538.
Frohlich, F., Moreira, K., Aguilar, P. S., Hubner, N. C., Mann, M., Walter, P. and Walther, T. C. (2009). A genome-wide screen for genes affecting eisosomes reveals Nce102 function in sphingolipid signaling. *J. Cell Biol.* **185**, 1227-1242.
Frohlich, F., Christiano, R., Olson, D. K., Alcazar-Roman, A., DeCamilli, P. and Walther, T. C. (2014). A role for eisosomes in maintenance of plasma membrane phosphoinositide levels. *Mol. Biol. Cell* **25**, 2797-2806.
Garciadeblas, B., Rubio, F., Quintero, F. J., Bañuelos, M. A., Haro, R. and Rodríguez-Navarro, A. (1993). Differential expression of two genes encoding isoforms of the ATPase involved in sodium efflux in Saccharomyces cerevisiae. *Mol. Gen. Genet.* **236**, 363-368.
Goddard, N. J., Dunn, M. A., Zhang, L., White, A. J., Jack, P. L. and Hughes, M. A. (1993). Molecular analysis and spatial expression pattern of a low-temperature-specific barley gene, blt101. *Plant Mol. Biol.* **23**, 871-879.
Grossmann, G., Malinsky, J., Stahlschmidt, W., Loibl, M., Weig-Meckl, I., Frommer, W. B., Opekarova, M. and Tanner, W. (2008). Plasma membrane microdomains regulate turnover of transport proteins in yeast. *J. Cell Biol.* **183**, 1075-1088.
Hammer, N. D., Wang, X., McGuffie, B. A. and Chapman, M. R. (2008). Amyloids: friend or foe? *J. Alzheimers Dis.* **13**, 407-419.
Huang, Z., Chen, K., Zhang, J., Li, Y., Wang, H., Cui, D., Tang, J., Liu, Y., Shi, X., Li, W. et al. (2013). A functional variomics tool for discovering drug-resistance genes and drug targets. *Cell Rep.* **3**, 577-585.
Inada, M., Ueda, A., Shi, W. M. and Takabe, T. (2005). A stress-inducible plasma membrane protein 3 (AcPMP3) in a monocotyledonous halophyte, Aneurolepidium chinense, regulates cellular Na+ and K+ accumulation under salt stress. *Planta* **220**, 395-402.
Ischebeck, T., Seiler, S. and Heilmann, I. (2010). At the poles across kingdoms: phosphoinositides and polar tip growth. *Protoplasma* **240**, 13-31.
Janke, C., Magiera, M. M., Rathfelder, N., Taxis, C., Reber, S., Maekawa, H., Moreno-Borchart, A., Doenges, G., Schwob, E., Schiebel, E. et al. (2004). A versatile toolbox for PCR-based tagging of yeast genes: new fluorescent proteins, more markers and promoter substitution cassettes. *Yeast* **21**, 947-962.
Johnson, L. V., Walsh, M. L., Bockus, B. J. and Chen, L. B. (1981). Monitoring of relative mitochondrial membrane potential in living cells by fluorescence microscopy. *J. Cell Biol.* **88**, 526-535.
Karotki, L., Huiskonen, J. T., Stefan, C. J., Ziolkowska, N. E., Roth, R., Surma, M. A., Krogan, N. J., Emr, S. D., Heuser, J., Grunewald, K. et al. (2011). Eisosome proteins assemble into a membrane scaffold. *J. Cell Biol.* **195**, 889-902.
Malathi, K., Higaki, K., Tinkelenberg, A. H., Balderes, D. A., Almanzar-Paramio, D., Wilcox, L. J., Erdeniz, N., Redican, F., Padamsee, M., Liu, Y. et al. (2004). Mutagenesis of the putative sterol-sensing domain of yeast Niemann Pick C-related protein reveals a primordial role in subcellular sphingolipid distribution. *J. Cell Biol.* **164**, 547-556.
Medina, J., Catalá, R. and Salinas, J. (2001). Developmental and stress regulation of RCI2A and RCI2B, two cold-inducible genes of arabidopsis encoding highly conserved hydrophobic proteins. *Plant Physiol.* **125**, 1655-1666.
Miyahara, K., Mizunuma, M., Hirata, D., Tsuchiya, E. and Miyakawa, T. (1996). The involvement of the Saccharomyces cerevisiae multidrug resistance transporters Pdr5p and Snq2p in cation resistance. *FEBS Lett.* **399**, 317-320.
Momoi, M., Tanoue, D., Sun, Y., Takematsu, H., Suzuki, Y., Suzuki, M., Suzuki, A., Fujita, T. and Kozutsumi, Y. (2004). SLI1 (YGR212W) is a major gene conferring resistance to the sphingolipid biosynthesis inhibitor ISP-1, and encodes an ISP-1 N-acetyltransferase in yeast. *Biochem. J.* **381**, 321-328.
Morsy, M. R., Almutairi, A. M., Gibbons, J., Yun, S. J. and de Los Reyes, B. G. (2005). The OsLti6 genes encoding low-molecular-weight membrane proteins are differentially expressed in rice cultivars with contrasting sensitivity to low temperature. *Gene* **344**, 171-180.
Moser von Filseck, J., Vanni, S., Mesmin, B., Antonny, B. and Drin, G. (2015). A phosphatidylinositol-4-phosphate powered exchange mechanism to create a lipid gradient between membranes. *Nat. Commun.* **6**, 6671.
Mottram, L. F., Forbes, S., Ackley, B. D. and Peterson, B. R. (2012). Hydrophobic analogues of rhodamine B and rhodamine 101: potent fluorescent probes of mitochondria in living C. elegans. *Beilstein J. Org. Chem.* **8**, 2156-2165.
Munkacsi, A. B., Chen, F. W., Brinkman, M. A., Higaki, K., Gutiérrez, G. D., Chaudhari, J., Layer, J. V., Tong, A., Bard, M., Boone, C. et al. (2011). An "exacerbate-reverse" strategy in yeast identifies histone deacetylase inhibition as a correction for cholesterol and sphingolipid transport defects in human Niemann-Pick type C disease. *J. Biol. Chem.* **286**, 23842-23851.
Murphy, E. R., Boxberger, J., Colvin, R., Lee, S. J., Zahn, G., Loor, F. and Kim, K. (2011). Pil1, an eisosome organizer, plays an important role in the recruitment of synaptojanins and amphiphysins to facilitate receptor-mediated endocytosis in yeast. *Eur. J. Cell Biol.* **90**, 825-833.
Nagiec, M. M., Wells, G. B., Lester, R. L. and Dickson, R. C. (1993). A suppressor gene that enables Saccharomyces cerevisiae to grow without making sphingolipids encodes a protein that resembles an Escherichia coli fatty acyltransferase. *J. Biol. Chem.* **268**, 22156-22163.
Navarre, C. and Goffeau, A. (2000). Membrane hyperpolarization and salt sensitivity induced by deletion of PMP3, a highly conserved small protein of yeast plasma membrane. *EMBO J.* **19**, 2515-2524.
Navarre, C., Ghislain, M., Leterme, S., Ferroud, C., Dufour, J. P. and Goffeau, A. (1992). Purification and complete sequence of a small proteolipid associated with the plasma-membrane H+-atpase of saccharomyces-cerevisiae. *J. Biol. Chem.* **267**, 6425-6428.
Navarre, C., Catty, P., Leterme, S., Dietrich, F. and Goffeau, A. (1994). 2 distinct genes encode small isoproteolipids affecting plasma-membrane H+-atpase activity of saccharomyces-cerevisiae. *J. Biol. Chem.* **269**, 21262-21268.
Nylander, M., Heino, P., Helenius, E., Tapio Palva, E., Ronne, H. and Welin, B. V. (2001). The low-temperature- and salt-induced RCI2A gene of Arabidopsis complements the sodium sensitivity caused by a deletion of the homologous yeast gene SNA1. *Plant Mol. Biol.* **45**, 341-352.
Obara, K., Sekito, T., Niimi, K. and Ohsumi, Y. (2008). The Atg18-Atg2 complex is recruited to autophagic membranes via phosphatidylinositol 3-phosphate and exerts an essential function. *J. Biol. Chem.* **283**, 23972-23980.
Olivera-Couto, A., Graña, M., Harispe, L. and Aguilar, P. S. (2011). The eisosome core is composed of BAR domain proteins. *Mol. Biol. Cell* **22**, 2360-2372.
Pfaffl, M. W. (2001). A new mathematical model for relative quantification in real-time RT-PCR. *Nucleic Acids Res.* **29**, e45.
Pokrzywa, W., Guerriat, B., Dodzian, J. and Morsomme, P. (2009). Dual Sorting of the Saccharomyces cerevisiae Vacuolar Protein Sna4p. *Eukaryot. Cell* **8**, 278-286.
Reggiori, F. and Pelham, H. R. B. (2001). Sorting of proteins into multivesicular bodies: ubiquitin-dependent and -independent targeting. *EMBO J.* **20**, 5176-5186.
Renard, H.-F., Demaegd, D., Guerriat, B. and Morsomme, P. (2010). Efficient ER exit and vacuole targeting of yeast Sna2p require two tyrosine-based sorting motifs. *Traffic* **11**, 931-946.
Ross, P. L., Huang, Y. N., Marchese, J. N., Williamson, B., Parker, K., Hattan, S., Khainovski, N., Pillai, S., Dey, S., Daniels, S. et al. (2004). Multiplexed protein quantitation in Saccharomyces cerevisiae using amine-reactive isobaric tagging reagents. *Mol. Cell. Proteomics* **3**, 1154-1169.
Rudge, S. A., Anderson, D. M. and Emr, S. D. (2004). Vacuole size control: regulation of PtdIns(3,5)P2 levels by the vacuole-associated Vac14-Fig4 complex, a PtdIns(3,5)P2-specific phosphatase. *Mol. Biol. Cell* **15**, 24-36.
Saarikangas, J., Zhao, H. and Lappalainen, P. (2010). Regulation of the actin cytoskeleton-plasma membrane interplay by phosphoinositides. *Physiol. Rev.* **90**, 259-289.
Schiestl, R. H. and Gietz, R. D. (1989). High efficiency transformation of intact yeast cells using single stranded nucleic acids as a carrier. *Curr. Genet.* **16**, 339-346.
Shah, Z. H., Jones, D. R., Sommer, L., Foulger, R., Bultsma, Y., D'Santos, C. and Divecha, N. (2013). Nuclear phosphoinositides and their impact on nuclear functions. *FEBS J.* **280**, 6295-6310.

Shetty, A., Swaminathan, A. and Lopes, J. M. (2013). Transcription regulation of a yeast gene from a downstream location. *J. Mol. Biol.* **425**, 457-465.
Shilov, I. V., Seymour, S. L., Patel, A. A., Loboda, A., Tang, W. H., Keating, S. P., Hunter, C. L., Nuwaysir, L. M. and Schaeffer, D. A. (2007). The Paragon Algorithm, a next generation search engine that uses sequence temperature values and feature probabilities to identify peptides from tandem mass spectra. *Mol. Cell. Proteomics.* **9**, 1638-1655.
Skaggs, B. A., Alexander, J. F., Pierson, C. A., Schweitzer, K. S., Chun, K. T., Koegel, C., Barbuch, R. and Bard, M. (1996). Cloning and characterization of the Saccharomyces cerevisiae C-22 sterol desaturase gene, encoding a second cytochrome P-450 involved in ergosterol biosynthesis. *Gene* **169**, 105-109.
Stawiecka-Mirota, M., Pokrzywa, W., Morvan, J., Zoladek, T., Haguenauer-Tsapis, R., Urban-Grimal, D. and Morsomme, P. (2007). Targeting of Sna3p to the endosomal pathway depends on its interaction with Rsp5p and multivesicular body sorting on its ubiquitylation. *Traffic* **8**, 1280-1296.
Stradalova, V., Stahlschmidt, W., Grossmann, G., Blazikova, M., Rachel, R., Tanner, W. and Malinsky, J. (2009). Furrow-like invaginations of the yeast plasma membrane correspond to membrane compartment of Can1. *J. Cell Sci.* **122**, 2887-2894.
Stradalova, V., Blazikova, M., Grossmann, G., Opekarová, M., Tanner, W. and Malinsky, J. (2012). Distribution of cortical endoplasmic reticulum determines positioning of endocytic events in yeast plasma membrane. *PLoS ONE* **7**, e35132.
Strømhaug, P. E., Reggiori, F., Guan, J., Wang, C.-W. and Klionsky, D. J. (2004). Atg21 is a phosphoinositide binding protein required for efficient lipidation and localization of Atg8 during uptake of aminopeptidase I by selective autophagy. *Mol. Biol. Cell* **15**, 3553-3566.
Suzuki, K., Kirisako, T., Kamada, Y., Mizushima, N., Noda, T. and Ohsumi, Y. (2001). The pre-autophagosomal structure organized by concerted functions of APG genes is essential for autophagosome formation. *EMBO J.* **20**, 5971-5981.
Suzuki, K., Akioka, M., Kondo-Kakuta, C., Yamamoto, H. and Ohsumi, Y. (2013). Fine mapping of autophagy-related proteins during autophagosome formation in Saccharomyces cerevisiae. *J. Cell Sci.* **126**, 2534-2544.
Szopinska, A., Degand, H., Hochstenbach, J. F., Nader, J. and Morsomme, P. (2011). Rapid response of the yeast plasma membrane proteome to salt stress. *Mol. Cell. Proteomics.* **11**, doi:10.1074/mcp.M111.009589
Tang, H.-Y., Xu, J. and Cai, M. (2000). Pan1p, End3p, and Sla1p, three yeast proteins required for normal cortical actin cytoskeleton organization, associate with each other and play essential roles in cell wall morphogenesis. *Mol. Cell. Biol.* **20**, 12-25.
Teste, M.-A., Duquenne, M., François, J. M. and Parrou, J.-L. (2009). Validation of reference genes for quantitative expression analysis by real-time RT-PCR in Saccharomyces cerevisiae. *BMC Mol. Biol.* **10**, 99.
Thevissen, K., Idkowiak-Baldys, J., Im, Y.-J., Takemoto, J., François, I. E. J. A., Ferket, K. K. A., Aerts, A. M., Meert, E. M. K., Winderickx, J., Roosen, J. et al. (2005). SKN1, a novel plant defensin-sensitivity gene in Saccharomyces cerevisiae, is implicated in sphingolipid biosynthesis. *FEBS Lett.* **579**, 1973-1977.
Walther, T. C., Brickner, J. H., Aguilar, P. S., Bernales, S., Pantoja, C. and Walter, P. (2006). Eisosomes mark static sites of endocytosis. *Nature* **439**, 998-1003.
Walther, T. C., Aguilar, P. S., Fröhlich, F., Chu, F., Moreira, K., Burlingame, A. L. and Walter, P. (2007). Pkh-kinases control eisosome assembly and organization. *EMBO J.* **26**, 4946-4955.
Wieker, H.-J., Kuschmitz, D. and Hess, B. (1987). Inhibition of yeast mitochondrial F1-ATPase, F0F1-ATPase and submitochondrial particles by rhodamines and ethidium bromide. *Biochim. Biophys. Acta* **892**, 108-117.
Yibmantasiri, P., Leahy, D. C., Busby, B. P., Angermayr, S. A., Sorgo, A. G., Boeger, K., Heathcott, R., Barber, J. M., Moraes, G., Matthews, J. H. et al. (2012). Molecular basis for fungicidal action of neothyonidioside, a triterpene glycoside from the sea cucumber, Australostichopus mollis. *Mol. Biosyst.* **8**, 902-912.
Young, M. E., Karpova, T. S., Brugger, B., Moschenross, D. M., Wang, G. K., Schneiter, R., Wieland, F. T. and Cooper, J. A. (2002). The Sur7p family defines novel cortical domains in Saccharomyces cerevisiae, affects sphingolipid metabolism, and is involved in sporulation. *Mol. Cell. Biol.* **22**, 927-934.
Zhao, C., Beeler, T. and Dunn, T. (1994). Suppressors of the Ca(2+)-sensitive yeast mutant (csg2) identify genes involved in sphingolipid biosynthesis. Cloning and characterization of SCS1, a gene required for serine palmitoyltransferase activity. *J. Biol. Chem.* **269**, 21480-21488.